

Giant Spin Pumping at Polymer/Ferromagnet Interfaces for Hybrid Spintronic Devices

Shiva Gaur¹, Akash Kumar^{2,3,4}, Himanshu Bangar⁵, Utkarsh Shashank²,
Hukum Singh¹, Saroj P. Dash⁵, Anubhav Raghav^{1*} and Johan Åkerman^{2,3,4*}

¹Department of Applied Sciences, The NorthCap University,
Gurugram, Haryana-122017, India

²Applied Spintronics Group, Department of Physics, University of Gothenburg, Fysikgränd 3,
412 96, Gothenburg, Sweden

³Research Institute of Electrical Communication, Tohoku University, 2-1-1 Katahira,
Aoba-ku, Sendai 980-8577 Japan

⁴Center for Science and Innovation in Spintronics, Tohoku University, 2-1-1 Katahira,
Aoba-ku, Sendai 980-8577 Japan

⁵Department of Microtechnology and Nanoscience, Chalmers University of Technology
412 96, Gothenburg, Sweden

*To whom correspondence should be addressed; E-mails:
anubhavraghav19292@gmail.com, johan.akerman@physics.gu.se

Abstract

While the growing utilization of polymers in flexible electronic devices has sparked significant interest in polymer/metal interfaces, spintronic studies of such interfaces remain limited. Here, we systematically study spin pumping across a polymer/ferromagnet metal interface between hydrogen silsesquioxane (HSQ) oligomer layers ($t_{HSQ} = 30, 36, 48$ nm) and NiFe ($t_{NiFe} = 4, 5, 7, 10$ nm) thin films. Using ferromagnetic resonance measurements, we observe strong spin pumping (large linewidth broadening) and a giant spin mixing conductance, reaching 19.8 nm^{-2} for HSQ = 48 nm, *i.e.* comparable to that of heavy metals. Our results suggest efficient spin transfer across the HSQ/NiFe interface, possibly originating from a combination of spin and orbital pumping, and provide valuable insights for designing self-powered and flexible spintronic devices utilizing polymers in combination with ferromagnetic materials.

1 Introduction

Over the past decades, spintronics has emerged as a promising technology to complement or even replace charge-based microelectronics, owing to its advantages such as non-volatility, low power consumption, high

speed, and radiation hardness [1]. A fundamental aspect of spintronic devices is charge-to-spin conversion, typically achieved via the spin Hall effect (SHE) in heavy metal/ferromagnet (HM/FM) bilayers [2, 3]. Conversely, spin pumping—the reciprocal effect of the SHE—transfers pure spin current from a precessing FM layer to a non-magnetic HM layer [4, 5]. This mechanism has been extensively employed for THz generation in FM/HM heterostructures [6] and for investigating spin transport phenomena at FM/non-magnetic interfaces, including those involving non-magnetic metals, two-dimensional materials, and topological insulators [7, 8, 9, 10]. However, significant spin pumping has primarily been observed in heavy metals with strong spin-orbit coupling, such as Pt, W, and Ta [11, 12, 13].

Recently, spin pumping has been extended to polymer-based systems, particularly organic materials, enabling the assessment of spin-orbit coupling and spin injection efficiency in these materials [14, 15, 16, 17]. Polymers are particularly attractive for spintronic applications due to their lightweight, flexibility, corrosion resistance, and environmental friendliness [18]. Significant research efforts have focused on interfacing polymers with ferromagnetic materials [19, 20, 21] to develop flexible spintronic devices [22] and explore the unique properties emerging from these hybrid systems [23, 24]. These advancements could lead to low-cost, potentially biocompatible spintronic devices [19] and enable integration with other technologies, such as solar cells [23], wearable healthcare applications, and polymer-based magneto-ionic systems [25].

Despite these advancements, a fundamental challenge remains: the large disparity in electrical conductivity when transferring spin currents from metallic FM layers to semiconducting, insulating, or polymer materials [26, 27]. This has led to skepticism regarding reports of significant spin pumping in such heterostructures [28]. However, recent experimental and theoretical studies suggest that orbital torque and orbital pumping—counterparts to spin-orbit torque and spin pumping—could play a crucial role [29]. Unlike the SHE, the orbital Hall effect (OHE) can be substantially stronger in lighter elements, including Si and 3d transition metals [30]. Moreover, the OHE is less affected by the large electrical conductivity mismatch at interfaces, making it a promising mechanism for overcoming spin injection limitations in semiconductors, insulators, and polymers. Building on previous observations of local orbital angular momentum in p-doped Si [31], as well as the inverse SHE and large anomalous Hall effect in Si [32, 33], silicon has re-emerged as a promising candidate for OHE and spintronics [34, 35]. While organic polymers have been explored in spintronics, silicon-based inorganic polymers remain largely unexplored, despite their abundance and unique properties [36].

In this work, we investigate the spin pumping behavior at the interface of a ferromagnetic metal (NiFe) and a silicon-based cross-linking polymer, hydrogen silsesquioxane (HSQ, $\text{H}_8\text{Si}_8\text{O}_{12}$). HSQ is a highly ordered oligomer widely used as a negative resist in photolithography and electron beam lithography [36, 37], as well as a planarizing interlayer dielectric film in integrated circuits [38]. By analyzing ferromagnetic resonance (FMR) linewidth broadening, we observed significant spin pumping from the NiFe layer into the non-magnetic HSQ polymer, as evidenced by a comparison with bare NiFe control samples. Systematic thickness-dependent studies of the ferromagnetic layer enabled us to determine the spin mixing conductance for various HSQ thicknesses, with the highest value, 19.8 nm^{-2} , observed for an HSQ thickness of 48 nm. This value exceeds those reported for other organic polymers [39, 40] and metal-free conjugated polymers [15], and is comparable to non-conjugated polymers [16, 17] and heavy metals with strong spin-orbit coupling, such as Ta, Pt, W, and Pd [11, 12, 41, 42].

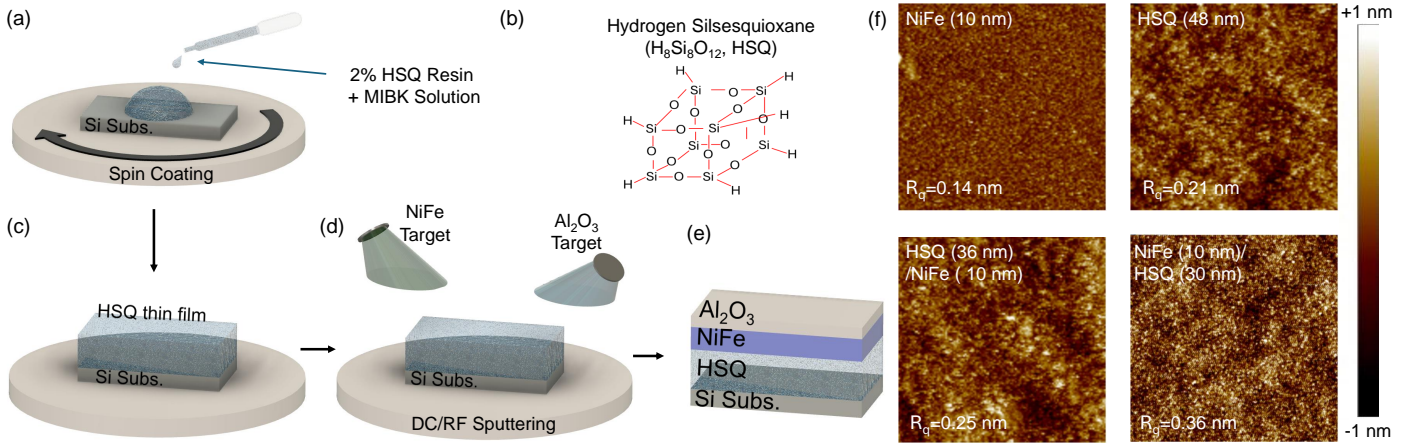


Figure 1: (a-e) Complete process of sample preparation; (a) Schematic depiction of preparing thin film of HSQ polymer using spin coating using HSQ resin solution, (b) the atomic structure of HSQ oligomer, (c) wet thin film of HSQ after spin coating (d) sputtering configuration for metal deposition (e) final thin film stack structures. (f) respective characterization with AFM over a $1 \times 1 \mu m^2$ scanning area of a bare NiFe (10 nm) thin film sample (without HSQ), HSQ thin film without ferromagnet NiFe, HSQ/NiFe stacks and reversed stack.

2 Results

2.1 Sample structure and characterization

Bilayer thin films of HSQ/NiFe were fabricated using a combination of spin coating and DC/RF magnetron sputtering, as illustrated in Fig. 1(a-e). HSQ is a low-dielectric inorganic oligomer with a cage-like structure composed of silicon and oxygen atoms with dangling hydrogen atoms (see Fig. 1b) [36, 43]. In solution, the oligomer forms amorphous SiO:H layers with excellent planarization properties [38]. Further details on sample preparation are provided in the Methods section.

The surface morphology of the HSQ thin films was characterized using atomic force microscopy (AFM) in tapping mode for four sample configurations: (i) pristine HSQ, (ii) HSQ after NiFe deposition, (iii) reference NiFe, and (iv) HSQ deposited on top of NiFe. The AFM topographic images in Fig. 1(f) reveal a homogeneous surface morphology across all samples, with no observable pinholes or significant surface irregularities. Quantitative analysis indicates that the average surface roughness varies from 0.14 nm for bare NiFe (10 nm) and 0.21 nm for HSQ (48 nm) to a maximum of 0.36 nm for the bilayer configuration of HSQ (30 nm)/NiFe (10 nm). These exceptionally low roughness values confirm that NiFe deposition has a negligible impact on the underlying HSQ layers [16]. Furthermore, the quality of the NiFe thin films deposited on HSQ remains largely preserved, underscoring the compatibility of the deposition process with spin-coated HSQ thin films.

To assess electrical properties, we measured the resistivity of HSQ/NiFe bilayers with NiFe (10 nm) for all HSQ thicknesses using the four-point probe technique (data provided in the Supplementary Information). The measured values are consistent with previously reported resistivities for NiFe thin films [44]. The reference sample (without HSQ) exhibited a lower resistivity compared to the HSQ-coated samples, which is attributed to the shunting effect in bare NiFe samples on semiconducting Si substrates [45]. This confirms that HSQ acts as an insulating layer.

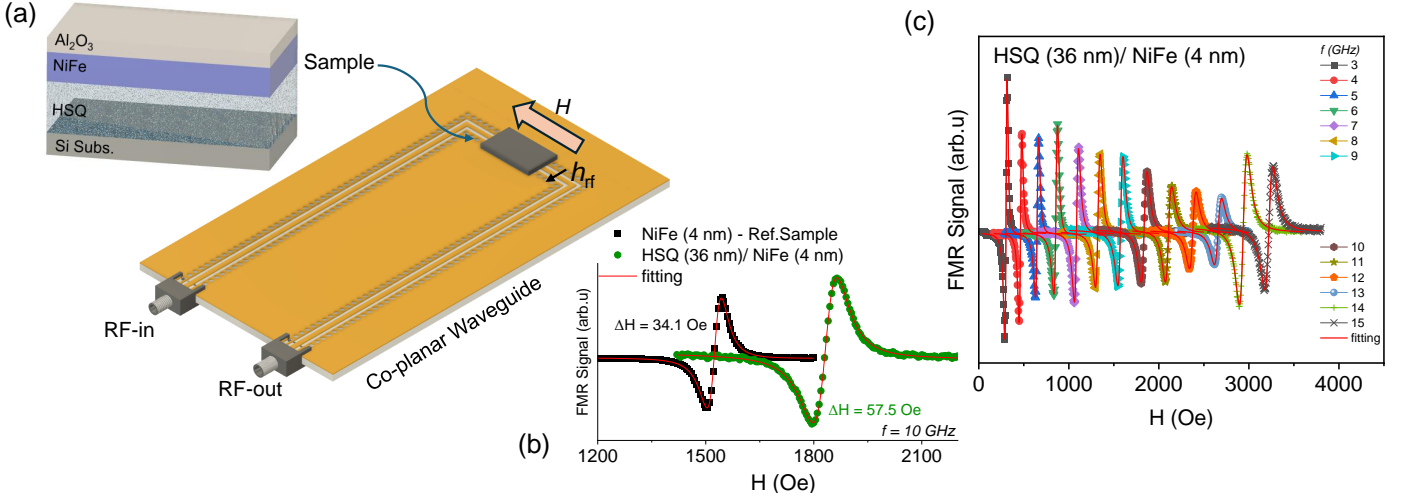


Figure 2: (a) Schematic of the ferromagnetic resonance (FMR) measurement geometry. (b) Comparison of the reference sample of NiFe (4 nm) and HSQ (36 nm)/NiFe(4 nm). (c) FMR signal for wide frequency range of 3-15 GHz for HSQ (36 nm)/NiFe (4 nm) thin film sample.

2.2 Spin pumping in HSQ/NiFe heterostructure: HSQ thickness dependence

To evaluate spin pumping at the HSQ/NiFe interface, FMR spectra were recorded for bilayer HSQ/NiFe films with varying HSQ thicknesses. The results were compared with reference NiFe films without HSQ. FMR measurements were performed using a NanOsc Phase-40 FMR instrument, and a schematic of the co-planar waveguide (CPW) with the static (H) and RF magnetic (h_{rf}) field directions is shown in Fig. 2a. Further details of the experimental setup can be found in [46, 47] and in the 'Methods' section. Fig. 2b compares the FMR spectra (linewidth and resonance field) of the HSQ (36 nm)/NiFe (4 nm) sample with the NiFe (4 nm) reference sample. Fig. 2c shows the frequency-dependent FMR spectra for the HSQ (36 nm)/NiFe (4 nm) film over the 3–15 GHz frequency range. Similar measurements were conducted for HSQ layers of 30, 36, and 48 nm with a 4 nm NiFe layer, as well as for the reference NiFe samples without HSQ. The raw spectra were analyzed by fitting them to a sum of symmetric and anti-symmetric Lorentzian derivative functions, following the method described in [41, 46]:

$$\frac{d\chi_{\text{FMR}}}{dH} \propto -\frac{2V_S\Delta(H - H_R)}{(\Delta H^2 + (H - H_R)^2)^2} + \frac{V_{AS}(\Delta H^2 - (H - H_R)^2)}{(\Delta H^2 + (H - H_R)^2)^2} \quad (1)$$

Here, V_S and V_{AS} represent the symmetric and anti-symmetric components. The applied field, linewidth, and resonance fields are represented by H , ΔH and H_R respectively.

The ΔH and H_R are extracted for all samples at different thicknesses for further calculations of the effective Gilbert damping (α_{eff}) and effective saturation magnetization (M_{eff}). The frequency-dependent ΔH and H_R curves for NiFe (4 nm) samples with varying HSQ thicknesses are shown in Fig. 3a and 3b. α_{eff} is extracted from the slope of linear fits of ΔH vs. frequency (Fig. 3a) using the following equation:

$$\Delta H = \Delta H_0 + \frac{2\pi\alpha_{\text{eff}}}{\gamma} f \quad (2)$$

Here, ΔH_0 indicates the inhomogeneous broadening and $\gamma = 29.6$ GHz/T the gyromagnetic ratio. Fits to Eq. 2 are shown as solid lines in Fig. 3a. ΔH_0 is found to be <12 Oe for all samples, confirming the high

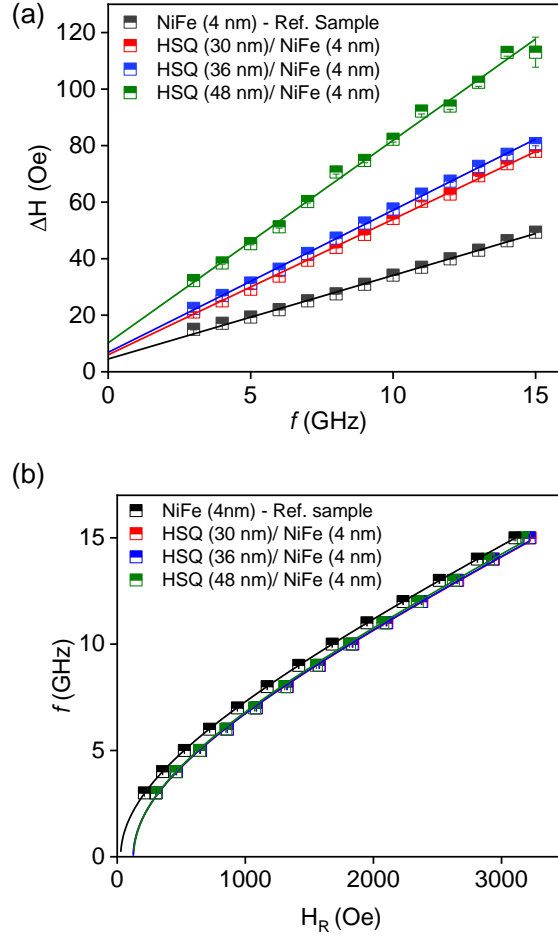


Figure 3: (a) Linewidth vs. frequency and (b) frequency vs. resonance field, for reference sample and other HSQ thicknesses with constant NiFe = 4 nm.

quality of NiFe thin films on top of HSQ. The increase in ΔH and its slope vs. frequency in the HSQ samples, compared to the reference samples, clearly indicates large spin pumping into the adjacent HSQ layer. We observed an 81% α_{eff} enhancement for HSQ(48 nm)/NiFe (4 nm) ($\alpha_{\text{eff}}=0.022$) as compared to the reference sample ($\alpha_{\text{eff}}=0.012$), highlighting the substantial spin pumping across the HSQ/NiFe interface.

Further, to calculate M_{eff} , f vs. H_R (Fig. 3b) is fitted using the Kittel formula [48]:

$$f = \frac{\gamma}{2\pi} \sqrt{(H_R + H_K)(H_R + H_K + 4\pi M_{\text{eff}})}, \quad (3)$$

where H_K represents the in-plane magnetic anisotropy constant. The frequency vs. H_R data for all HSQ thicknesses are found to be consistent with similar effective magnetization values, again showing the uniformity of NiFe thin films grown on HSQ.

2.3 Ferromagnet thickness dependence and spin mixing conductance

Fig. 4a presents the effective damping coefficient (α_{eff}) as a function of the inverse NiFe thickness for all HSQ thicknesses ($t_{\text{HSQ}} = 0, 30, 36, \text{ and } 48 \text{ nm}$). While the increase in damping with HSQ thickness could arise from mechanisms such as spin memory loss [27, 49] and two-magnon scattering [50], the linear dependence

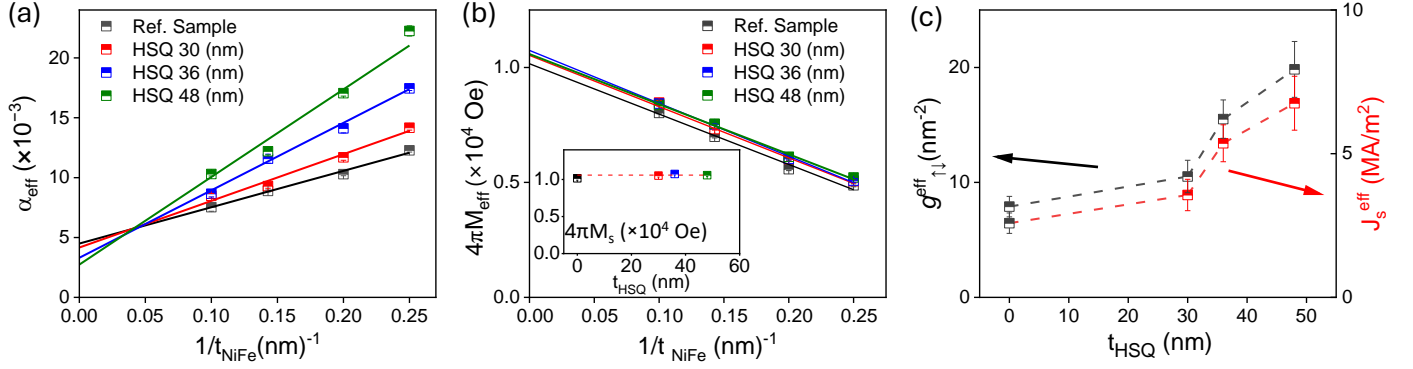


Figure 4: (a) Effective Gilbert damping vs. the inverse of NiFe thickness ($1/t_{\text{NiFe}}$) for all samples. (b) Saturation Magnetization ($4\pi M_s$) vs. inverse thickness of NiFe, inset shows the saturation magnetization for HSQ thickness i.e the intercept of Fig. (b). (c) The resultant spin mixing conductance and spin current density parameter vs. HSQ thickness ($t_{\text{HSQ}}=0$ nm represents the reference NiFe sample without HSQ), calculated using Eq. (4) and (5).

of linewidth on frequency (Fig. 3a) rules out significant contributions from two-magnon scattering or phonon drag [50, 51]. The observed linear increase in α_{eff} with the inverse ferromagnet thickness suggests minimal spin memory loss at the interface, confirming HSQ as an efficient spin sink [4, 10, 27, 46].

To quantify the spin pumping efficiency, we determine the effective spin mixing conductance ($g_{\text{eff}}^{\uparrow\downarrow}$) by fitting α_{eff} vs. $1/t_{\text{NiFe}}$ using the following equation [41]:

$$\alpha_{\text{eff}} = \alpha_0 + \gamma \hbar \frac{g_{\text{eff}}^{\uparrow\downarrow}}{4\pi M_s t_{\text{NiFe}}} \quad (4)$$

Here, α_0 represents the intrinsic Gilbert damping (bulk) of NiFe, and \hbar is the reduced Planck's constant. The saturation magnetization ($4\pi M_s$), obtained from a linear fit of M_{eff} vs. $1/t_{\text{NiFe}}$ [see Fig. 4(b)], is found to be approximately 1.05 T for all sample series [inset of Fig. 4(b)]. Fig. 4c summarizes $g_{\text{eff}}^{\uparrow\downarrow}$ for different HSQ thicknesses, with a dotted black line as a visual guide. The extracted values are $g_{\text{eff}}^{\uparrow\downarrow} = 7.9 \pm 0.8$, 10.5 ± 1.4 , 15.5 ± 1.6 , and $19.8 \pm 2.4 \text{ nm}^{-2}$ for the reference, 30 nm, 36 nm, and 48 nm HSQ samples, respectively.

The lower $g_{\text{eff}}^{\uparrow\downarrow}$ in the reference sample is attributed to minimal spin pumping into the substrate and the AlO_x capping layer. The intrinsic damping values (α_0) for all samples range from 0.0030 to 0.0045, aligning with previously reported NiFe values [52]. Interestingly, samples with HSQ exhibit *lower* α_0 than the reference NiFe, potentially due to the formation of a thin silicide layer at the Si/NiFe interface [53].

To further analyze spin transport, we calculated the spin current density (J_s^{eff}) using the following equation [54]:

$$J_s^{\text{eff}} = \frac{2e}{\hbar} \times \frac{\hbar\omega}{4\pi} \mathbf{g}_{\uparrow\downarrow} \sin^2 \theta_C \times \frac{2\omega [M_s \gamma + \sqrt{(M_s \gamma)^2 + (2\omega)^2}]}{(M_s \gamma)^2 + (2\omega)^2}, \quad (5)$$

Here, e represents the electron charge, and ω is the angular frequency. The magnetization precession cone angle, θ_C , is given by $\theta_C = \frac{h_{\text{rf}}}{2\Delta H}$, where h_{rf} is the strength of the RF field experienced by the sample. The final

term, $\frac{2\omega[M_s\gamma + \sqrt{(M_s\gamma)^2 + (2\omega)^2}]}{(M_s\gamma)^2 + (2\omega)^2}$, represents an ellipticity correction factor, which accounts for the ellipticity of the magnetization precession.

The calculated values of J_s^{eff} are plotted in Fig.4c (indicated by the red visual guide) and exhibit a similar trend as $g_{\text{eff}}^{\uparrow\downarrow}$. Moreover, the J_s^{eff} values are comparable to those observed at FM/HM interfaces, such as Co/Pt and NiFe/Ta [41, 55], confirming the generation of a significant spin current in the HSQ/NiFe heterostructures.

2.4 Reversed sample structures: NiFe/HSQ heterostructure

Notably, both $g_{\text{eff}}^{\uparrow\downarrow}$ and J_s^{eff} increase with HSQ thickness, indicating a large spin diffusion length in HSQ thin films and confirming the bulk nature of the polymer as a spin sink. However, measurements for thicker HSQ films were not feasible, as they require a more viscous HSQ resin solution in MIBK, which leads to significant surface degradation and increased interfacial roughness.

To verify that the observed effects are not caused by permanent modifications to the HSQ thin films due to high-energy bombardment during sputtering, we fabricated samples with a reversed stack order: NiFe thin films were first deposited on HiR-Si substrates via DC sputtering, followed by spin coating of HSQ thin films. The process was carried out with minimal delay to prevent NiFe oxidation.

Fig. 5 presents the effective Gilbert damping as a function of HSQ thickness, with NiFe thickness fixed at 10 nm. The continuous increase in effective Gilbert damping with increasing HSQ thickness further confirms the bulk nature of spin pumping in HSQ thin films, ruling out any structural or interfacial degradation. Additionally, this result demonstrates that the quality of the HSQ layer remains unchanged regardless of its deposition order relative to NiFe.

2.5 Comparison with HSQ/CoFeB interface

To determine whether spin pumping is exclusive to NiFe, we fabricated an additional sample series with CoFeB thin films: HiR-Si Subs./HSQ (30, 36, 48 nm)/CoFeB (4 nm)/Al₂O₃ (4 nm) along with a reference sample HiR-Si Subs./CoFeB (4 nm)/Al₂O₃ (4 nm). FMR measurements for varying HSQ thickness (data in supplementary information) revealed a trend similar to that observed in the HSQ/NiFe and NiFe/HSQ systems.

Compared to the 81% enhancement reported above for HSQ/NiFe, we observed an even higher 95% increase in effective Gilbert damping for HSQ (48 nm)/CoFeB, compared to its reference ($\alpha_{\text{eff}} = 0.0094$ vs. 0.0048). This further supports our results and confirms the bulk nature of spin pumping in HSQ thin films regardless of the details of the ferromagnetic metal. The linewidth vs. frequency data and effective Gilbert damping as a function of HSQ thickness are provided in the supplementary figures.

3 Discussion

Earlier studies on FM/organic semiconductor polymer interfaces have also demonstrated significant spin pumping and spin mixing conductance. The organic semiconductors interfaced with NiFe thin films exhibit “spinter-

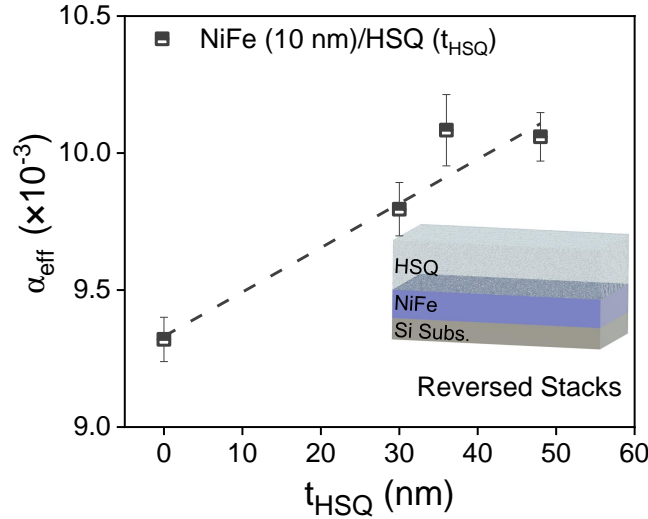


Figure 5: Effective Gilbert damping vs. HSQ thickness for the reversed stack, with fixed $t_{\text{NiFe}}=10$ nm. The dotted line shows a guide to the eye.

face" effects, where interaction-induced spin-dependent density of states influences spin transport [56, 57, 58]. Recent studies on conjugated polymers [15, 20, 39, 40] further confirm strong spin pumping effects.

Talluri et al. [39] reported $g_{\text{eff}}^{\uparrow\downarrow} = 1.54 \text{ nm}^{-2}$ for perylene diimide (PDI)/NiFe, while Gupta et al. found $g_{\text{eff}}^{\uparrow\downarrow} \approx 1.02 \text{ nm}^{-2}$ for a pyrene oligomer/NiFe system. In another work, Vetter et al. [15] investigated P3MT (polymethylthiophene conjugated polymer brush) and P3HT (poly3-hexylthiophene) as non-magnetic layers in NiFe-based heterostructures. Their results showed that the out-of-plane columnar arrangement in P3MT enhanced the damping, yielding $g_{\text{eff}}^{\uparrow\downarrow} = 1.06 \times 10^{21} \text{ m}^{-2}$, nearly two orders of magnitude higher than conventional metallic and semiconductor systems ($10^{18}\text{--}10^{19} \text{ m}^{-2}$). For P3HT, they reported $g_{\text{eff}}^{\uparrow\downarrow} = 4.22 \times 10^{20} \text{ m}^{-2}$. Additionally, Wittmann et al. [40] examined spin pumping in a small molecule based on DNTT – dinaphtho[2, 3 – b : 2, 3, f]thieno[3, 2 – b]thiophene with NiFe, reporting $g_{\text{eff}}^{\uparrow\downarrow} = 3.35 \text{ nm}^{-2}$ for DNTT, 2.98 nm^{-2} for Ph-DNTT-Ph, and 0.63 nm^{-2} for C8-DNTT-C8, demonstrating the influence of molecular structure on spin injection efficiency.

Materials	$g_{\text{eff}}^{\uparrow\downarrow} \text{ (nm}^{-2}\text{)}$	Reference
Heavy Metals	1–30	[12, 13, 41]
PTEO	11.8	Tahir et al. [17]
PVEO	32	Tahir et al. [16]
DNTT	3.35	Wittmann et al. [40]
Ph-DNTT-Ph	2.98	Wittmann et al. [40]
C8-DNTT-C8	0.63	Wittmann et al. [40]
P3HT*	0.42×10^3	Vetter et al. [15]
P3MT*	1.06×10^3	Vetter et al. [15]
PDI	1.54	Talluri et al. [39]
Pyrene	1.02	Gupta et al. [20]
HSQ	19.8	This Work

Table 1: Comparison of spin mixing conductance ($g_{\text{eff}}^{\uparrow\downarrow}$) for various materials. The P3HT and P3MT represent the $g_{\text{eff}}^{\uparrow\downarrow}$ at infinite polymer thicknesses [15].

In recent studies, Tahir et al. [16, 17] investigated non-conjugated paramagnetic radical polymers, PTEO and PVEO, as efficient spin sources, reporting $g_{\text{eff}}^{\uparrow\downarrow} = 11.8$ and 32.0 nm^{-2} , respectively—values significantly higher than those observed in heavy metals. In our study, HSQ (48 nm) thin films exhibit $g_{\text{eff}}^{\uparrow\downarrow} = 19.83 \pm 2.43 \text{ nm}^{-2}$, nearly an order of magnitude higher than previously reported conjugated polymers [20, 39, 40] and comparable to values reported in [16, 17].

Table 1 summarizes the $g_{\text{eff}}^{\uparrow\downarrow}$ values reported for various polymer/ferromagnet interfaces. Notably, these $g_{\text{eff}}^{\uparrow\downarrow}$ values are comparable to those of conventional heavy metals such as Pt, W, and Ta, which are well known for their strong spin-orbit coupling and spin Hall effect [12, 13, 41]. This finding highlights the potential of polymers as efficient spin conductors. A benchmarking of $g_{\text{eff}}^{\uparrow\downarrow}$ across different material classes is provided in the supplementary information.

High spin pumping and large $g_{\text{eff}}^{\uparrow\downarrow}$ are typically found in metallic non-magnets interfaced with ferromagnets that have similar electrical resistivity, clean interfaces, and strong spin-orbit coupling [11, 27]. In contrast, insulating non-magnets present a fundamental block for spin injection from metallic ferromagnets [26]. Since HSQ is an insulating material with weak spin-orbit coupling, conventional mechanisms would predict weak or negligible spin pumping. However, as discussed earlier, the linear increase of $g_{\text{eff}}^{\uparrow\downarrow}$ with HSQ thickness suggests a bulk spin-sink behavior and a high spin diffusion length.

One possible explanation for the unexpectedly large $g_{\text{eff}}^{\uparrow\downarrow}$ could be a significant contribution from, or even a dominant role of, orbital pumping [59, 60] at the NiFe/HSQ interface. Recent studies have reported orbital pumping and orbital torques with long relaxation lengths in light elements and oxide materials with low spin-orbit coupling when interfaced with ferromagnets, such as Ti [29] and CuO_x [61]. Additionally, Si has been predicted [31] and more recently confirmed [35] to exhibit a large orbital angular moment, further supporting our argument.

Hence, we propose that the large effective spin pumping observed in our samples may originate from a *combination* of spin and orbital pumping—i.e., spin-orbital pumping—although further detailed measurements and theoretical analysis are required to fully understand this mechanism. Overall, our results confirm a significant spin-pumping effect and establish HSQ as an efficient non-magnetic spin sink layer. Our study also highlights the potential of inorganic polymers for achieving large spin pumping, opening new opportunities in energy harvesting from photovoltaic polymers [23, 24] and in the development of flexible spintronic devices for memory and wearable healthcare applications [25].

4 Conclusion

In summary, we investigated the magnetodynamic response of HSQ/NiFe thin films and demonstrated significant spin pumping from NiFe into the HSQ layer, as evidenced by linewidth broadening and increased effective Gilbert damping. Our findings provide strong experimental support for efficient spin injection into HSQ, a silicon-based inorganic polymer. The spin injection efficiency, quantified by the effective spin mixing conductance, was determined to be 19.8 nm^{-2} for a 48 nm thick HSQ thin film, which is remarkably high and comparable to values reported for heavy metals with strong spin-orbit coupling. Given that HSQ is an insulating material with inherently low spin-orbit coupling, our results suggest that orbital pumping may play a dominant role in spin transport at the NiFe/HSQ interface. Further theoretical and experimental investigations are necessary to fully elucidate the contribution of orbital effects in HSQ-based spintronic systems.

Beyond its fundamental implications, our study establishes HSQ as a promising non-magnetic spin sink for next-generation spintronic applications. The possibility of achieving efficient spin transport in an inorganic polymer opens new avenues for flexible and energy-efficient spintronic devices. Future research could explore the integration of HSQ-based heterostructures into energy harvesting technologies and wearable electronics.

Methods

Sample Preparation

The bilayer thin films of HSQ/NiFe were prepared using a combination of spin coating and DC/RF magnetron sputtering (See Fig. 1a-e). First, the polymer hydrogen silsesquioxane (HSQ, $\text{H}_8\text{Si}_8\text{O}_{12}$) was spin-coated onto high-resistivity silicon (HiR-Si) substrates. We deposit these polymer thin films using 2% HSQ resin solution in methyl isobutyl ketone (MIBK) solution, the low viscosity of the solution gives higher uniformity. No pre or post-annealing treatment were performed. The HSQ solution (2% HSQ in MIBK) was spin-coated under optimized conditions to achieve film thicknesses of 30, 36, and 48 nm. Following this, NiFe thin films with varying thicknesses (4, 5, 7, and 10 nm) were deposited using DC/RF magnetron sputtering. The sputtering was conducted in an ultra-high vacuum chamber (AJA Orion 8) with a base pressure of 4×10^{-8} mbar. The deposition of NiFe thin films was carried out with a DC power of 50 W and a low deposition rate of 1.4 Å/s to avoid potential damage to the HSQ layer. All films were capped with a 3 nm Al_2O_3 layer to prevent oxidation.

Four sets of samples were prepared for spin-pumping analysis: (i) a reference set of NiFe thin films without HSQ, (ii) HiR-Si/HSQ/NiFe bilayers, (iii) a reversed stack where NiFe was deposited first, followed by immediate HSQ spin-coating to minimize oxidation, and (iv) a control set of HSQ-coated Si substrates with no NiFe layer. The varying thickness HSQ-coated substrates, along with bare Si substrates, were placed in the sputtering chamber together to ensure consistent NiFe/ Al_2O_3 thin films. All samples were fabricated under identical deposition rates to ensure consistency across the series. Surface characterization, presented in Fig. 1f, was performed using atomic force microscopy (AFM) in tapping mode with a Bruker Dimension Icon system.

Atomic Force Microscopy

Atomic force microscopy (AFM) has been done using high resolution Bruker Dimension ICON system to examine the surface morphology in tapping mode under ambient conditions. The scans were conducted over an area of $5 \times 5 \mu\text{m}^2$ and $1 \times 1 \mu\text{m}^2$ with a pixel size of 512×512 pixels. The obtained AFM images were analyzed using Nanoscope analysis software to obtain the roughness values. The root mean square roughness was found from the range of 0.12-0.36 nm, which confirms uniformity and defect free nature of the thin films which ultimately supports the high quality of the stacks.

Ferromagnetic Resonance

Ferromagnetic resonance (FMR) measurements were performed to investigate the magnetodynamical properties using a coplanar waveguide (CPW)-based NanOsc PhaseFMR-40 setup. The FMR measurements were

carried out at room temperature over a frequency range of 3–15 GHz with an in-plane external magnetic field. The sample was positioned downward (flip-chip), i.e., with the deposited layers facing the CPW. An electromagnet was used to produce an external magnetic field ($\mu_0 H$) of up to 1 T. A small frequency (98 Hz) field modulation was employed with the Helmholtz coil (biased with an integrated Helmholtz coil source in the instrument) to boost the signal-to-noise ratio. All measurements were performed at ambient temperature to ensure reproducibility.

Supporting Information

Supporting Information file is available from the corresponding author.

Acknowledgment

S.G. and H.S. acknowledge the Central Research Facility at The NorthCap University, Gurugram for its instrumental and financial support. J.Å. acknowledges funding from the Knut and Alice Wallenberg Foundation (Dnr. KAW 2022.0079) and as a Swedish Research Council Distinguished Professor (Dnr. 2024-01943).

Conflict of Interest

The authors declare no conflict of interest.

Author Contributions

S.G., A.K., A.R. and J.Å. initiated the idea and planned the study. S.G. prepared the thin films, obtained experimental data and performed the FMR analysis with input from all authors. H.B. performed the AFM measurements. S.G. wrote the original draft of the paper. A.K., A.R. and J.Å. coordinated and supervised the work. All authors contributed to the data analysis and co-wrote the manuscript.

References

- [1] Bernard Dieny, Ioan Lucian Prejbeanu, Kevin Garello, Pietro Gambardella, Paulo Freitas, Ronald Lehn-dorff, Wolfgang Raberg, Ursula Ebels, Sergej O Demokritov, Johan Akerman, et al. Opportunities and challenges for spintronics in the microelectronics industry. *Nat. Electron.*, 3(8):446–459, 2020.
- [2] JE Hirsch. Spin hall effect. *Phys. Rev. Lett.*, 83(9):1834, 1999.
- [3] Jairo Sinova, Sergio O Valenzuela, Jörg Wunderlich, CH Back, and T Jungwirth. Spin hall effects. *Rev. Mod. Phys.*, 87(4):1213–1260, 2015.
- [4] Yaroslav Tserkovnyak, Arne Brataas, and Gerrit EW Bauer. Enhanced gilbert damping in thin ferromag-netic films. *Phys. Rev. Lett.*, 88(11):117601, 2002.
- [5] Yaroslav Tserkovnyak, Arne Brataas, Gerrit EW Bauer, and Bertrand I Halperin. Nonlocal magnetization dynamics in ferromagnetic heterostructures. *Rev. Mod. Phys.*, 77(4):1375–1421, 2005.

- [6] Tom Seifert, S Jaiswal, U Martens, J Hannegan, Lukas Braun, Pablo Maldonado, F Freimuth, A Kronenberg, J Henrizi, I Radu, et al. Efficient metallic spintronic emitters of ultrabroadband terahertz radiation. *Nat. Photon.*, 10(7):483–488, 2016.
- [7] Y Kajiwara, K Harii, S Takahashi, Jun-ichiro Ohe, K Uchida, M Mizuguchi, H Umezawa, H Kawai, Kazuya Ando, K Takanashi, et al. Transmission of electrical signals by spin-wave interconversion in a magnetic insulator. *Nature*, 464(7286):262–266, 2010.
- [8] Paul Noël, Felix Trier, Luis M Vicente Arche, Julien Bréhin, Diogo C Vaz, Vincent Garcia, Stéphane Fusil, Agnès Barthélémy, Laurent Vila, Manuel Bibes, et al. Non-volatile electric control of spin–charge conversion in a srtio₃ rashba system. *Nature*, 580(7804):483–486, 2020.
- [9] Rajni Bansal, Akash Kumar, Niru Chowdhury, Naveen Sisodia, Arun Barvat, Anjana Dogra, Prabir Pal, and PK Muduli. Extrinsic spin-orbit coupling induced enhanced spin pumping in few-layer mos₂/py. *J. Magn. Mater.*, 476:337–341, 2019.
- [10] Himanshu Bangar, Akash Kumar, Niru Chowdhury, Richa Mudgal, Pankhuri Gupta, Ram Singh Yadav, Samaresh Das, and Pranaba Kishor Muduli. Large spin-to-charge conversion at the two-dimensional interface of transition-metal dichalcogenides and permalloy. *ACS Appl. Mater. Interfaces*, 14(36):41598–41604, 2022.
- [11] Kazuya Ando, Y Kajiwara, S Takahashi, S Maekawa, K Takemoto, M Takatsu, and E Saitoh. Angular dependence of inverse spin–hall effect induced by spin pumping investigated in a ni₈₁fe₁₉/pt thin film. *Phys. Rev. B*, 78(1):014413, 2008.
- [12] Hiroyasu Nakayama, Kazuya Ando, Kazuya Harii, Tatsuro Yoshino, Ryo Takahashi, Yosuke Kajiwara, Ken-ichi Uchida, Yasunori Fujikawa, and Eiji Saitoh. Geometry dependence on inverse spin hall effect induced by spin pumping in ni₈₁fe₁₉/pt films. *Phys. Rev. B*, 85(14):144408, 2012.
- [13] Deepika Jhajhria, Nilamani Behera, Dinesh K Pandya, and Sujeet Chaudhary. Dependence of spin pumping in w/cofeb heterostructures on the structural phase of tungsten. *Phys. Rev. B*, 99(1):014430, 2019.
- [14] Jagannath Devkota, Rugang Geng, Ram Chandra Subedi, and Tho Duc Nguyen. Organic spin valves: a review. *Adv. Funct. Mater.*, 26(22):3881–3898, 2016.
- [15] Eric Vetter, Ian VonWald, Shijia Yang, Liang Yan, Sanaz Koohfar, Divine Kumah, Zhi-Gang Yu, Wei You, and Dali Sun. Tuning of spin-orbit coupling in metal-free conjugated polymers by structural conformation. *Phys. Rev. Mater.*, 4(8):085603, 2020.
- [16] Hamas Tahir, Kangying Liu, Yun-Fang Yang, Kaushik Baruah, Brett M Savoie, and Bryan W Boudouris. Verdazyl radical polymers for advanced organic spintronics. *Nat. Commun.*, 16(1):652, 2025.
- [17] Hamas Tahir, Carsten Flores-Hansen, Sheng-Ning Hsu, Zihao Liang, Jayant Naga, Neil R Dilley, Brett M Savoie, and Bryan W Boudouris. Spintronic pathways in a nonconjugated radical polymer glass. *Adv. Mater.*, 37(3):2406727, 2025.
- [18] Lidan Guo, Xianrong Gu, Xiangwei Zhu, and Xiangnan Sun. Recent advances in molecular spintronics: multifunctional spintronic devices. *Adv. Mater.*, 31(45):1805355, 2019.
- [19] Shahriar Mostufa, Shuang Liang, Vinit Kumar Chugh, Jian-Ping Wang, and Kai Wu. Spintronic devices for biomedical applications. *npj Spintronics*, 2(1):26, 2024.

- [20] Ritu Gupta, Jhantu Pradhan, Arabinda Haldar, Chandrasekhar Murapaka, and Prakash Chandra Mondal. Chemical approach towards broadband spintronics on nanoscale pyrene films. *Angew. Chem.*, 135(35):e202307458, 2023.
- [21] Ismael G Serrano, Jaganandha Panda, Fernand Denoel, Orjan Vallin, Dibya Phuyal, Olof Karis, and M Venkata Kamalakar. Two-dimensional flexible high diffusive spin circuits. *Nano letters*, 19(2):666–673, 2019.
- [22] Giuseppe Muscas, Petra E Jönsson, Ismael G Serrano, Örjan Vallin, and M Venkata Kamalakar. Ultralow magnetostrictive flexible ferromagnetic nanowires. *Nanoscale*, 13(12):6043–6052, 2021.
- [23] Chunlei Li, Yaojin Li, Yifan Zhao, Yujing Du, Meng Zhao, Wanjun Peng, Yangyang Wu, Ming Liu, and Ziyao Zhou. Sunlight control of ferromagnetic damping in photovoltaic/ferromagnetic heterostructures. *Adv. Funct. Mater.*, 32(16):2111652, 2022.
- [24] Lidan Guo, Shunhua Hu, Xianrong Gu, Rui Zhang, Kai Wang, Wenjing Yan, and Xiangnan Sun. Emerging spintronic materials and functionalities. *Adv. Mater.*, 36(22):2301854, 2024.
- [25] Rohit Pachat, Djoudi Ourdani, Maria-Andromachi Syskaki, Alessio Lamperti, Subhajit Roy, Song Chen, Adriano Di Pietro, Ludovic Largeau, Roméo Juge, Maryam Massouras, et al. Magneto-ionics in annealed w/cofeb/hfo2 thin films. *Adv. Mater. Interfaces*, 9(36):2200690, 2022.
- [26] G Schmidt, D Ferrand, LW Molenkamp, AT Filip, and BJ Van Wees. Fundamental obstacle for electrical spin injection from a ferromagnetic metal into a diffusive semiconductor. *Phys. Rev. B*, 62(8):R4790, 2000.
- [27] J-C Rojas-Sánchez, N Reyren, P Laczkowski, W Savero, J-P Attané, C Deranlot, M Jamet, J-M George, Laurent Vila, and H Jaffrès. Spin pumping and inverse spin hall effect in platinum: the essential role of spin-memory loss at metallic interfaces. *Phys. Rev. Lett.*, 112(10):106602, 2014.
- [28] Bin Lu, Yue Niu, Qian Chen, Ping Kwan Johnny Wong, Qingjie Guo, Wei Jiang, Ashutosh Rath, Stephen J Pennycook, Lei Wang, Ke Xia, et al. Is semiconducting transition-metal dichalcogenide suitable for spin pumping? *Nano Lett.*, 25(1):35–40, 2024.
- [29] Hiroki Hayashi, Dongwook Go, Satoshi Haku, Yuriy Mokrousov, and Kazuya Ando. Observation of orbital pumping. *Nat. Electron.*, 7(8):646–652, 2024.
- [30] Giacomo Sala and Pietro Gambardella. Giant orbital hall effect and orbital-to-spin conversion in 3 d, 5 d, and 4 f metallic heterostructures. *Phys. Rev. Research*, 4(3):033037, 2022.
- [31] B Andrei Bernevig, Taylor L Hughes, and Shou-Cheng Zhang. Orbitronics: The intrinsic orbital current in p-doped silicon. *Phys. Rev. Lett.*, 95(6):066601, 2005.
- [32] Ncholu Manyala, Yvan Sidis, John F DiTusa, Gabriel Aeppli, David P Young, and Zachary Fisk. Large anomalous hall effect in a silicon-based magnetic semiconductor. *Nat. Mater.*, 3(4):255–262, 2004.
- [33] Kazuya Ando and Eiji Saitoh. Observation of the inverse spin hall effect in silicon. *Nat. Commun.*, 3(1):629, 2012.
- [34] Insu Baek and Hyun-Woo Lee. Negative intrinsic orbital hall effect in group xiv materials. *Phys. Rev. B*, 104(24):245204, 2021.

- [35] Ryoga Matsumoto, Ryo Ohshima, Yuichiro Ando, Dongwook Go, Yuriy Mokrousov, and Masashi Shi-raishi. Observation of giant orbital hall effect in si. *arXiv preprint arXiv:2501.14237*, 2025.
- [36] Feng Jin, Jie Liu, Yuan-Yuan Zhao, Xian-Zi Dong, Mei-Ling Zheng, and Xuan-Ming Duan. $\lambda/30$ inorganic features achieved by multi-photon 3d lithography. *Nat. Commun.*, 13(1):1357, 2022.
- [37] M Peuker, MH Lim, Henry I Smith, R Morton, AK van Langen-Suurling, J Romijn, EWJM van der Drift, and FCMJM Van Delft. Hydrogen silsesquioxane, a high-resolution negative tone e-beam resist, investigated for its applicability in photon-based lithographies. *Microelectron. Eng.*, 61:803–809, 2002.
- [38] Chang-Chung Yang and Wen-Chang Chen. The structures and properties of hydrogen silsesquioxane (hsq) films produced by thermal curing. *J. Mater. Chem.*, 12(4):1138–1141, 2002.
- [39] Talluri Manoj, Srinu Kotha, Bibekananda Paikaray, Dasari Srideep, Arabinda Haldar, Kotagiri Venkata Rao, and Chandrasekhar Murapaka. Giant spin pumping at the ferromagnet (permalloy)–organic semiconductor (perylene diimide) interface. *RSC Adv.*, 11(56):35567–35574, 2021.
- [40] Angela Wittmann, Guillaume Schweicher, Katharina Broch, Jiri Novak, Vincent Lami, David Cornil, Erik R McNellis, Olga Zadvorna, Deepak Venkateshvaran, Kazuo Takimiya, et al. Tuning spin current injection at ferromagnet-nonmagnet interfaces by molecular design. *Phys. Rev. Lett.*, 124(2):027204, 2020.
- [41] Akash Kumar, Rajni Bansal, Sujeet Chaudhary, and Pranaba Kishor Muduli. Large spin current generation by the spin hall effect in mixed crystalline phase ta thin films. *Phys. Rev. B*, 98(10):104403, 2018.
- [42] K Ando, J Ieda, K Sasage, S Takahashi, S Maekawa, and E Saitoh. Electric detection of spin wave resonance using inverse spin-hall effect. *Appl. Phys. Lett.*, 94(26), 2009.
- [43] Hyun Wook Ro and Christopher L Soles. Silsesquioxanes in nanoscale patterning applications. *Mater. Today*, 14(1-2):20–33, 2011.
- [44] Hamid Mazraati, Mohammad Zahedinejad, and Johan Åkerman. Improving the magnetodynamical properties of nife/pt bilayers through hf dusting. *Appl. Phys. Lett.*, 113(9), 2018.
- [45] Nilamani Behera, Avinash Kumar Chaurasiya, Victor H González, Artem Litvinenko, Lakhman Bainsla, Akash Kumar, Roman Khymyn, Ahmad A Awad, Himanshu Fulara, and Johan Åkerman. Ultra-low current 10 nm spin hall nano-oscillators. *Advanced Materials*, 36(5):2305002, 2024.
- [46] Lakhman Bainsla, Akash Kumar, Ahmad A Awad, Chunlei Wang, Mohammad Zahedinejad, Nilamani Behera, Himanshu Fulara, Roman Khymyn, Afshin Houshang, Jonas Weissenrieder, et al. Ultrathin ferrimagnetic gdfeco films with low damping. *Adv. Funct. Mater.*, 32(23):2111693, 2022.
- [47] Shiva Gaur, Nilamani Behera, Johan Åkerman, and Anubhav Raghav. Spin pumping in moderately perpendicular w/cofeb/hfo_x thin films. *Spin*, 14(02):2340022, 2024.
- [48] Charles Kittel. On the theory of ferromagnetic resonance absorption. *Phys. Rev.*, 73(2):155, 1948.
- [49] Frédéric Bonell, Minori Goto, Guillaume Sauthier, Juan F Sierra, Adriana I Figueroa, Marius V Costache, Shinji Miwa, Yoshishige Suzuki, and Sergio O Valenzuela. Control of spin–orbit torques by interface engineering in topological insulator heterostructures. *Nano Lett.*, 20(8):5893–5899, 2020.

- [50] Rodrigo Arias and DL Mills. Extrinsic contributions to the ferromagnetic resonance response of ultrathin films. *Phys. Rev. B*, 60(10):7395, 1999.
- [51] Yang Li, Yan Li, Rui Sun, Jia-nan Liu, Na Li, Xu Yang, Zi-zhao Gong, Zong-kai Xie, Wei He, Xiang-qun Zhang, et al. Drag effect induced large anisotropic damping behavior in magnetic thin films with strong magnetic anisotropy. *J. Phys. Condens. Matter.*, 33(17):175801, 2021.
- [52] Nobuyuki Inaba, Hironori Asanuma, Satoshi Igarashi, Shunnsuke Mori, Fumiyoshi Kirino, Kunihiro Koike, and Hiroaki Morita. Damping constants of ni-fe and ni-co alloy thin films. *IEEE Trans. Magn.*, 42(10):2372–2374, 2006.
- [53] Frank Schulz, Robert Lawitzki, Hubert Głowiński, Filip Lisiecki, Nick Träger, Piotr Kuświk, Eberhard Goering, Gisela Schütz, and Joachim Gräfe. Increase of gilbert damping in permalloy thin films due to heat-induced structural changes. *J. Appl. Phys.*, 129(15), 2021.
- [54] O Mosendz, V Vlaminc, JE Pearson, FY Fradin, GEW Bauer, SD Bader, and A Hoffmann. Detection and quantification of inverse spin hall effect from spin pumping in permalloy/normal metal bilayers. *Phys. Rev. B*, 82(21):214403, 2010.
- [55] Akash Kumar, Nidhi Pandey, Dileep Kumar, Mukul Gupta, Sujeet Chaudhary, and Pranaba Kishor Muduli. Influence of annealing on spin pumping in sputtered deposited co/pt bilayer thin films. *Physica B: Condensed Matter*, 570:254–258, 2019.
- [56] Mirko Cinchetti, V Alek Dediu, and Luis E Hueso. Activating the molecular spinterface. *Nat. Mater.*, 16(5):507–515, 2017.
- [57] Stefano Sanvito. The rise of spinterface science. *Nat. Phys.*, 6(8):562–564, 2010.
- [58] Esita Pandey, Purbasha Sharangi, Antarjami Sahoo, Swayang Priya Mahanta, Srijani Mallik, and Subhankar Bedanta. A perspective on multifunctional ferromagnet/organic molecule spinterface. *Applied Physics Letters*, 123(4), 2023.
- [59] Dongwook Go, Kazuya Ando, Armando Pezo, Stefan Blügel, Aurélien Manchon, and Yuriy Mokrousov. Orbital pumping by magnetization dynamics in ferromagnets. *arXiv preprint arXiv:2309.14817*, 2023.
- [60] Armando Pezo, Andrés Saul, Aurélien Manchon, and Rémi Arras. Spin and orbital rashba effects at the ni/hfo ₂ interface. *arXiv preprint arXiv:2412.04927*, 2024.
- [61] Shilei Ding, Hanchen Wang, William Legrand, Paul Noël, and Pietro Gambardella. Mitigation of gilbert damping in the co₂/cuo x orbital torque system. *Nano Lett.*, 24(33):10251–10257, 2024.